

Experimental research based on robot-assisted surgery: Lower limb fracture reduction surgery planning navigation system

Hanwen Du^{1,2}  | Geyang Wu^{1,3} | Ying Hu¹ | Yucheng He^{1,4}  | Peng Zhang¹

¹Shenzhen Institute of Advanced Technology, Chinese Academy of Sciences, Shenzhen, China

²University of Chinese Academy of Sciences, Beijing, China

³Harbin Institute of Technology, Shenzhen, Shenzhen, China

⁴Guangzhou Medical University, Guangzhou, China

Correspondence

Yucheng He and Peng Zhang, Shenzhen Institute of Advanced Technology, Chinese Academy of Sciences.

Email: yuchenghe@gzhmu.edu.cn and zhangpeng@siat.ac.cn

Funding information

Regional Joint Fund of Guangdong, Grant/Award Number: 2021B1515130003; Shenzhen Key Laboratory of Minimally Invasive Surgical Robotics and System, Grant/Award Number: ZDSYS201707271637577; Key Fundamental Research Program of Shenzhen, Grant/Award Number: JCYJ20220818101412026; Basic and Applied Basic Research Foundation of Guangdong Province, Grant/Award Number: 2022A1515010574; Shenzhen Science and Technology Program, Grant/Award Number: JCYJ20210324101012031

Abstract

Background and Aims: Lower extremity fracture reduction surgery is a key step in the treatment of lower extremity fractures. How to ensure high precision of fracture reduction while reducing secondary trauma during reduction is a difficult problem in current surgery.

Methods: First, segmentation and three-dimensional reconstruction are performed based on fracture computed tomography images. A cross-sectional point cloud extraction algorithm based on the normal filtering of the long axis of the bone is designed to obtain the cross-sectional point clouds of the distal bone and the proximal bone, and the optimal reset target pose of the broken bone is obtained by using the iterative closest point algorithm. Then, the optimal reset sequence of reset parameters was determined, combined with the broken bone collision detection algorithm, a surgical planning algorithm for lower limb fracture reset was proposed, which can effectively reduce the reset force while ensuring the accuracy of the reset process without collision.

Results: The average error of the reduction of the model bone was within 1.0 mm. The reduction operation using the planning and navigation system of lower extremity fracture reduction surgery can effectively reduce the reduction force. At the same time, it can better ensure the smooth change of the reduction force.

Conclusion: Planning and navigation system of lower extremity fracture reduction surgery is feasible and effective.

KEYWORDS

lower extremity fracture reduction, point cloud extraction, surgical navigation, surgical planning

This is an open access article under the terms of the [Creative Commons Attribution-NonCommercial-NoDerivs](https://creativecommons.org/licenses/by-nc-nd/4.0/) License, which permits use and distribution in any medium, provided the original work is properly cited, the use is non-commercial and no modifications or adaptations are made.

© 2024 The Authors. *Health Science Reports* published by Wiley Periodicals LLC.

1 | INTRODUCTION

At present, the computer-assisted planning system for surgery has become an important tool for surgeons.^{1,2} The important steps of the surgical planning system are generally to input the medical image of the patient's lesion, segment the medical image, determine the surgical approach, determine the size and design of the surgical instrument or prosthesis, perform the surgical simulation in the navigation system, and finally support the entire surgical navigation system completes real clinical operations.³⁻⁵

In spinal surgery, Ferrero et al.⁶ proposed a three-dimensional (3D) surgical planning software, SpineEOS, which combines stereoscopic radiological images to assist users in preoperative planning. Knez et al.,⁷ Qi et al.,⁸ and others proposed a surgical planning method for spinal curvature treatment through 3D reconstruction of vertebrae and shape simulation of vertebral screws, which increased the degree of vertebral screw fixation and greatly improved the treatment effect. In joint replacement surgery, Miura et al.,⁹ Gao et al.,¹⁰ and others proposed the Zed knee joint system, which can help users perform preoperative planning for total knee arthroplasty surgery. For hip-related surgery, Sugano¹¹ proposed a nonimaging computer-assisted navigation system for total hip arthroplasty. Even though there is no actual hip reduction experiment, the postoperative effect of different femoral neck lengths can be seen through the system. The data of the operation can also be stored in the system to complete the simulated hip replacement operation.

For fracture reduction surgery, Frnstahl et al.¹² proposed a computer-assisted fracture reconstruction method based on the contralateral bone mirror model. This method uses the healthy contralateral bone as a template and cooperates with GPU registration calculations to complete surgical planning. For complex proximal humerus fractures, it minimizes user interaction and planning time compared to manual reduction planning. Han et al.,¹³ Zhao et al.,¹⁴ and others proposed a surgical planning system based on multibody 3D registration in pelvic fracture surgery, which reduced image registration errors and fracture reduction errors. Liu proposed a semiautomatic fracture damage measurement system for comminuted fractures of the tibia,¹⁵ which performed a 3D reconstruction of the fracture by defining the degree of fracture damage to complete the reduction plan. Lee proposed an optical tracking system-free image-guided semiautomatic registration master-slave robotic system for long bone fracture surgery, which can eliminate the line-of-sight limitation of image-guided robotic surgery and increase the rotation angle of the traditional Stewart platform workspace.¹⁶

At present, there are few systematic studies of the planning system for lower limb fracture reduction surgery. Due to the diversity of lower limb fractures and the difficulty of reduction, and the fracture process also involves the reduction force generated by the soft tissues,^{17,18} excessive reduction surgery can easily cause secondary damage to the soft tissues at the fracture site.¹⁹ Some

studies on fracture surgery planning use the method of using the contralateral bone generation prediction model to complete the reduction. Some systems use deep learning or statistics to build bone models.²⁰⁻²² This system also needs to be more heavily dependent on the quantity and quality of healthy bone data. Therefore, research on surgical planning for lower extremity fracture reduction still needs to be developed and improved.

This study aims to develop a planning and navigation system for lower extremity fracture surgery. While ensuring accurate registration and tracking, it can also complete preoperative fracture reduction planning and intraoperative visual assistance, which can effectively improve the reduction accuracy of fracture sections. It also addresses the problem of secondary soft tissue damage at the fracture site caused by excessive resetting force.

The main contributions of this study are as follows: (1) The method of extracting the sectional point cloud using the long axis of the bone and the normal angle is proposed. This method extracts more points, reduces the effect of missing matching points on the alignment, and improves the stability of the alignment of distal and proximal bones. (2) A detailed analysis of the reduction force was performed to determine the optimal reduction sequence for the reduction parameters. Based on this, a fracture reduction path planning algorithm was designed and implemented to avoid interosseous collision and reduce reduction force.

2 | MATERIALS AND METHODS

2.1 | Medical image segmentation and reconstruction of lower extremity fractures and registration of fracture planes

In this section, after segmentation and reconstruction of the original medical image of the lower extremity fracture, the point cloud model of the broken bone is first obtained by point cloud sampling, and the bone long axis normal filtering method is designed to extract the point cloud of the fracture section. The position and attitude change from the fracture state to the reset state were obtained through point cloud registration.

2.1.1 | Medical fracture image reconstruction and point cloud sampling

The region growing segmentation algorithm and the watershed segmentation algorithm have been used in combination to obtain relatively pure fracture regions.^{23,24} 3D reconstruction of 2D medical tomography images based on VTK using the marching cube algorithm.²⁵ The point cloud model is then obtained by uniform sampling. Figure 1 shows the results of uniform sampling of the model bone.

2.1.2 | Bone long axis normal filtering method to extract cross-sectional point cloud

In this study, the method of the angle between the long axis of the bone and the normal line is used to extract the cross-sectional point cloud. This method will extract more points, which can reduce the negative effect of loss of matching points caused by gaps and other reasons, and the impact on registration will be less.

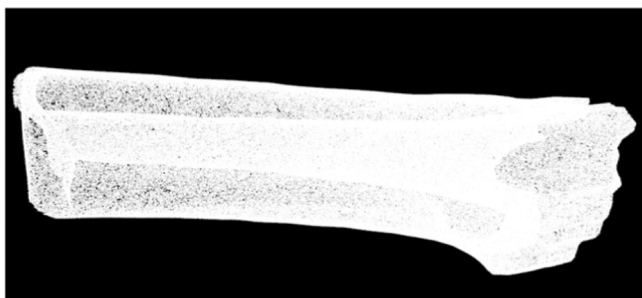


FIGURE 1 Broken bone model point cloud sampling.

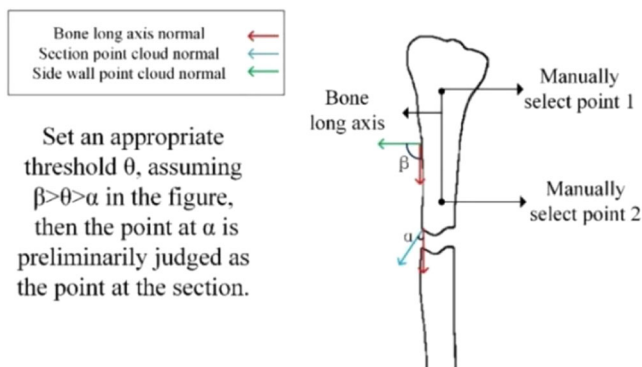


FIGURE 2 Select the bone long axis.

In this method, the long axis of the bone is a vector representing the axial direction of the lower limb bone. The position of the long axis of the bone is not fixed and can be selected flexibly. The number of points in the point cloud is large, and fractures will cause a relatively obvious angle between the cross-section and the bone side wall. The randomness of manually selecting the long axis of the bone has a small impact on the registration, when determining the long axis of the bone, two points on the side of the bone can be manually selected to generate the long axis of the bone. As shown in Figure 2, manually select two points on the side of the bone to obtain the long axis l of the bone.

Because the lower extremity bone is approximately cylindrical, the normal of most points on the bone sidewall point cloud is approximately perpendicular to the direction of the long axis of the bone. In contrast, while the angle between the normal of the points on the fracture section and the direction of the long axis of the bone is small. This feature can be used to classify the point cloud by setting an appropriate empirical threshold. Points with an angle greater than the threshold are considered to be on the sidewall. Otherwise, they are on the cross-section as shown in Figure 3.

Use kd-tree to search and traverse the point cloud, get the adjacent point set of each point, and use the point set to fit the plane through the least square method to get the normal vector of the point. The angle between the normal of the broken bone model point and the direction of the long axis can be obtained by calculating the cosine value of the angle by the equation:

$$\cos \theta = \frac{\mathbf{v}_i \times \mathbf{l}}{\|\mathbf{l}\| \sqrt{(v_{ix})^2 + (v_{iy})^2 + (v_{iz})^2}} \quad (1)$$

Combined with Figure 3B, it can be seen that when the value of ϵ_θ is 60, the cross-section point cloud can be separated. In actual operation, the ϵ_θ value can be manually modified to meet different

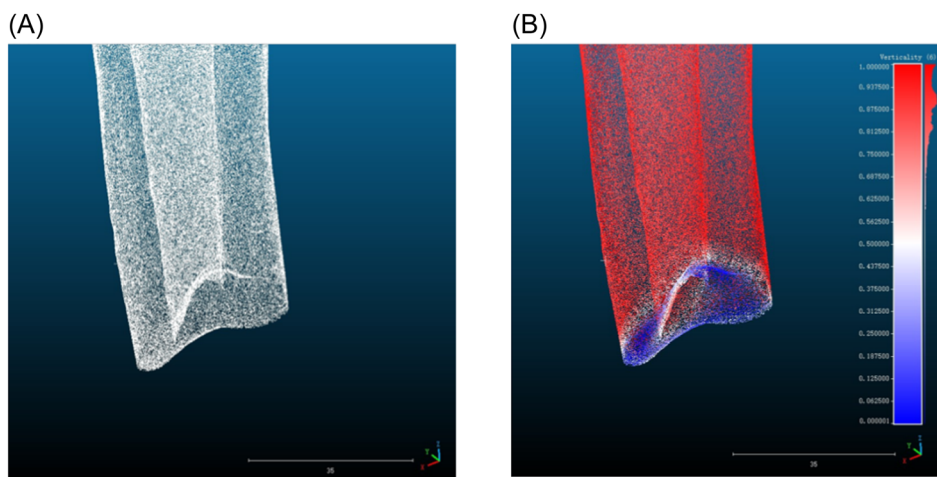


FIGURE 3 Angle change between the normal of the fracture point cloud and the long axis of the bone. (A) Origin cloud model. (B) Angle change between normal and long axis (angle 0°–90° corresponds to verticality 0–1).

types of broken bones. By setting the threshold ϵ_θ , traverse the entire bone model point cloud according to the kd-tree search method, and keep the points of $|\theta| < \epsilon_\theta$ in the point cloud, so as to obtain the filtered cross-sectional point cloud, as shown in Figure 4.

After extracting the section point cloud, there will be an error point cloud and some outlier noise points similar to the nature of the section, the system will automatically remove abnormal noise points. This study adopts the method of point cloud clustering and bilateral filtering to eliminate these outliers. The actual effect of section extraction and outlier processing on a fractured bone point cloud model is shown in Figure 5.

2.1.3 | Cross-section point cloud registration using ICP algorithm

In this study, the ICP algorithm is used to achieve the matching and alignment of the sections, taking advantage of the fact that the fracture sections are originally on the same plane. Starting from a random or given initial correspondence, the algorithm continuously iteratively finds the optimal correspondence between point clouds to compute the pose transformation of two sets of point clouds.



FIGURE 4 Bone long axis normal method to extract cross-sectional point cloud.

The actual registration point cloud and registration results are shown in Figure 6, where the yellow, blue, and green point clouds represent the source point cloud, target point cloud, and point cloud after registration respectively. It can be observed that the registered point cloud almost coincides with the target point cloud that is, the cross-sectional registration alignment is completed.

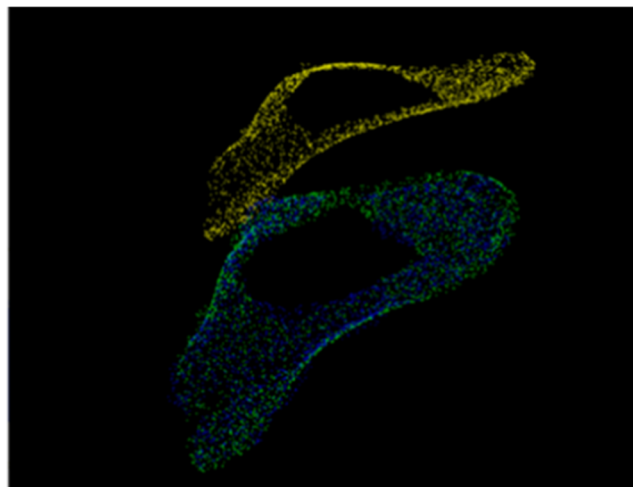


FIGURE 6 Cross-section point cloud registration.

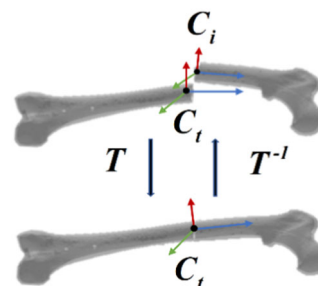


FIGURE 7 Schematic diagram of the relationship between the original coordinate system and the target coordinate system.

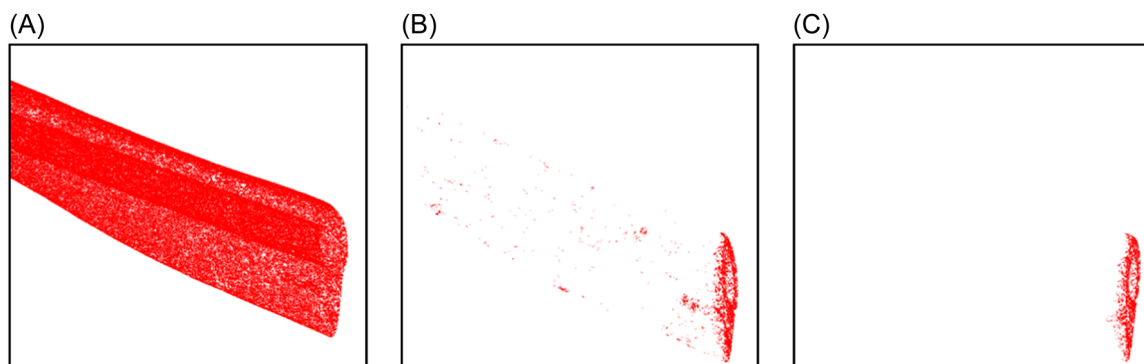


FIGURE 5 Effect of outlier processing. (A) Raw point cloud. (B) Point cloud after section extraction. (C) Point cloud after outlier processing.

TABLE 1 Fracture reduction parameter table.

Parameter	Describe	Calculation expression
t_s (mm)	s axis displacement parameter	T'_{14}
t_t (mm)	t axis displacement parameter	T'_{24}
t_l (mm)	Displacement parameter along the long axis of the bone	T'_{34}
α (°)	The angle of rotation parameter around the s axis	$\alpha = \text{atan2}\left(\frac{T'_{32}}{\cos \beta}, \frac{T'_{33}}{\cos \beta}\right)$
β (°)	The angle of rotation parameter around the t axis	$\beta = -\text{asin}(T'_{31})$
γ (°)	The angle of rotation parameter about the long axis of the bone	$\gamma = \text{atan2}\left(\frac{T'_{21}}{\cos \beta}, \frac{T'_{11}}{\cos \beta}\right)$

2.2 | Lower extremity fracture repositioning path planning algorithm

This section mainly studies the planning of the reset path. First, the parameters of the reset path planning algorithm are determined, and then the interbone collision and reset force are studied separately, and the corresponding interbone collision detection algorithm and the optimal reset process sequence are designed. Integrate a safer and more effective reduction path planning algorithm for lower extremity fracture reduction surgery.

2.2.1 | Determine algorithm parameters for reset path planning

To complete the planning in the coordinate system established by the computed tomography (CT) image, it is necessary to establish the coordinate system before and after the fracture reduction in the reconstructed 3D space coordinate system to determine the planning parameters of the fracture reduction. In the clinical surgical treatment of lower limb fractures, stretching, traction and manual reduction are achieved by displacing the distal, the coordinate systems are re-established on the proximal broken bone and the distal broken bone, respectively, to obtain the posture transformation of the distal bone during the reduction process.

\mathbf{v}_1 and \mathbf{v}_2 are the normal vectors of any two points, and the unit vector orthogonal to them is taken as the bone long axis l_{12} .

$$l_{12} = \frac{\mathbf{v}_1 \times \mathbf{v}_2}{\|\mathbf{v}_1 \times \mathbf{v}_2\|}. \quad (2)$$

The normal vector of the point cloud is randomly divided into two sets with the number of elements k , and the best bone long axis direction l is obtained by traversing the two sets:

$$l = \frac{1}{n} \sum_{i=1, j=1}^k \frac{\mathbf{v}_i \times \mathbf{v}_j}{\|\mathbf{v}_i \times \mathbf{v}_j\|}. \quad (3)$$

The other two axes in the coordinate system are perpendicular to l . Using the long axis l' of the other end bone as a reference, select the

**FIGURE 8** Bone collision detection.

second coordinate axis, that is, the direction vector perpendicular to the plane composed of the two fractured bones, defined as t ; determine the third coordinate axis s according to the rule of the Cartesian rectangular coordinate system, As shown in the following formula:

$$t = l \times l', \quad (4)$$

$$s = l \times t. \quad (5)$$

This results in the complete target Cartesian coordinate system:

$$C_t = \begin{bmatrix} s & t & l & o \\ 0 & 0 & 0 & 1 \end{bmatrix}. \quad (6)$$

Let the homogeneous coordinate transformation matrix obtained by cross-sectional registration be T , after taking the inverse, the original position of the distal bone before reduction can be obtained through the coordinate system of the target position.

$$C_i = T^{-1} \cdot C_t. \quad (7)$$

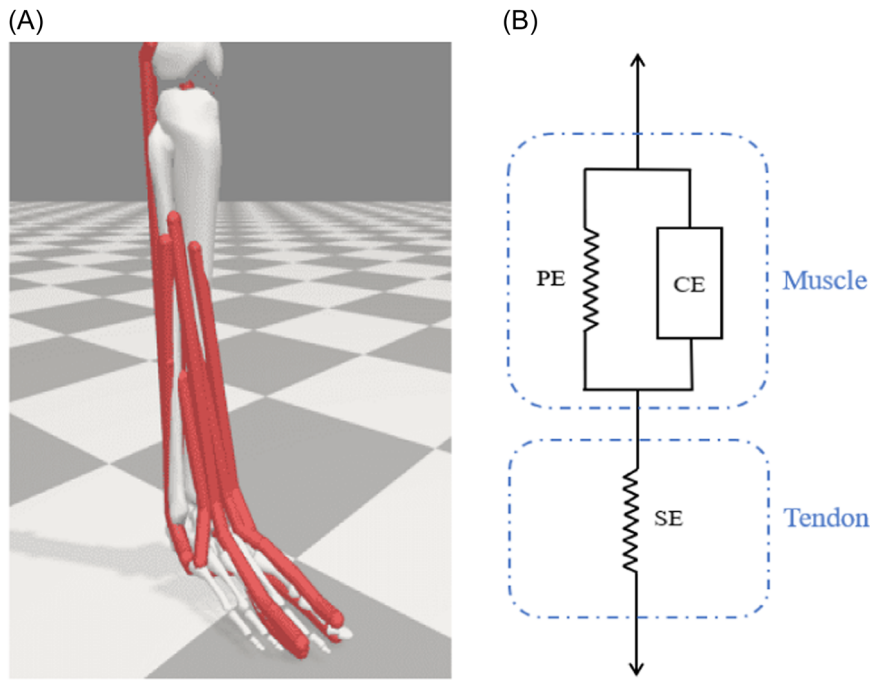


FIGURE 9 Muscle model. (A) Calf skeletal muscle model. (B) Muscle-tendon unit. CE, contraction unit; PE, parallel unit; SE, series unit.

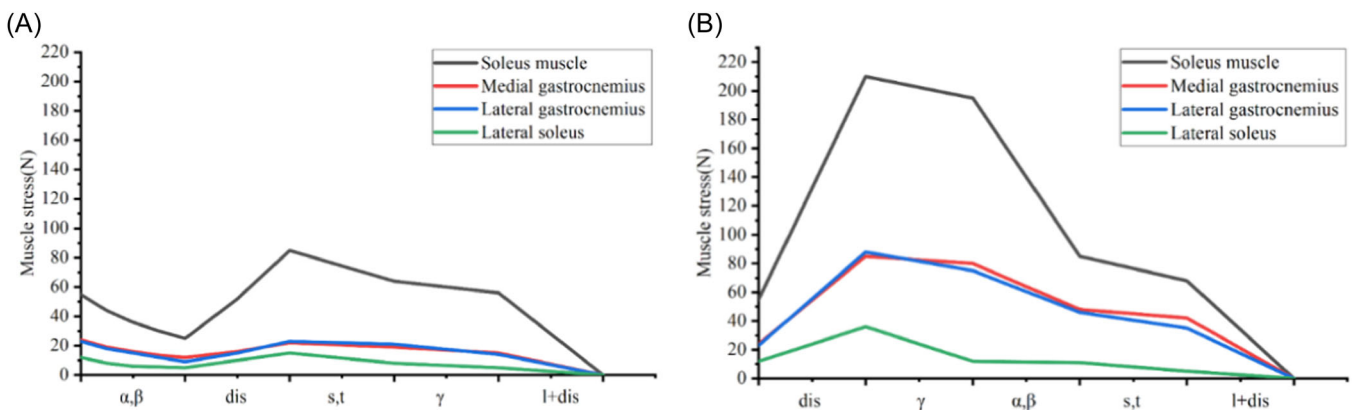


FIGURE 10 Passive stress of muscles under different reset sequences. (A) Reset sequence ($\alpha, \beta \rightarrow \text{dis} \rightarrow s, t \rightarrow \gamma \rightarrow 1 + \text{dis}$). (B) Reset sequence ($\text{dis} \rightarrow \gamma \rightarrow \alpha, \beta \rightarrow s, t \rightarrow 1 + \text{dis}$).

In this way, the relationship between the target coordinate system after reset, the original coordinate system before reset, and the coordinate transformation matrix obtained by section registration is obtained, as shown in Figure 7.

In this study, the three position parameters and three angle parameters of the relative coordinate system are used as the basis for adjustment, which is consistent with the clinical technique of lower extremity fracture reduction.

First, based on the target coordinate system C_t , obtain the relative homogeneous transformation matrix T' of the coordinate system

$$T' = C_t^{-1} \cdot C_i \quad (8)$$

That is, in the target coordinate system, the distal bone moves to the initial position of the distal bone through the coordinate

transformation matrix T' , and the position parameters in the relative position transformation matrix are the values that need to be adjusted for each parameter in the reset and reverse process. The corresponding translation amount in T' is the corresponding translation parameter t_s , t_t , and t_l . The angle parameters α , β , and γ need to be calculated by the rotation matrix T' in \mathbf{R} to obtain Euler angles, and the process of rotating around the α , β , and γ axes successively is selected for calculation. All fracture reduction parameters obtained and their descriptions are shown in Table 1.

2.2.2 | Bone collision detection algorithm design

In the fracture reduction planning process, the corresponding interosseous collision detection algorithm is designed to ensure that the planned

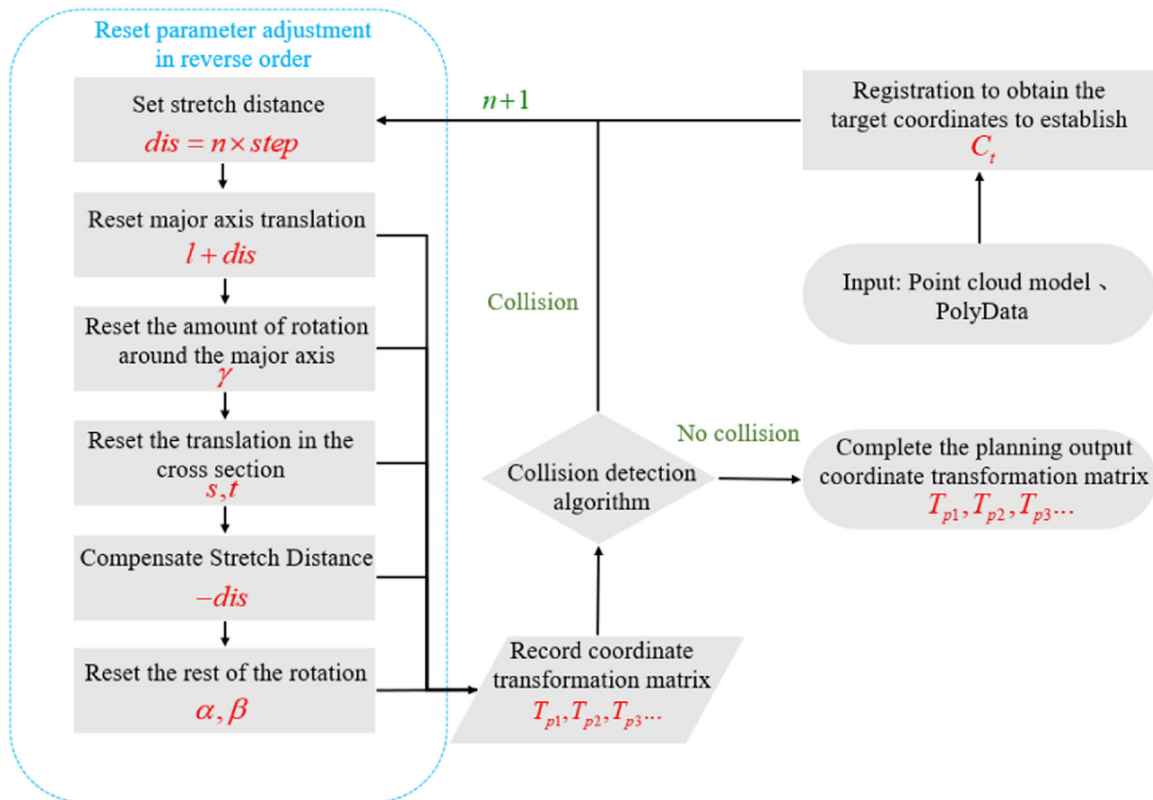


FIGURE 11 Reset planning algorithm flowchart.

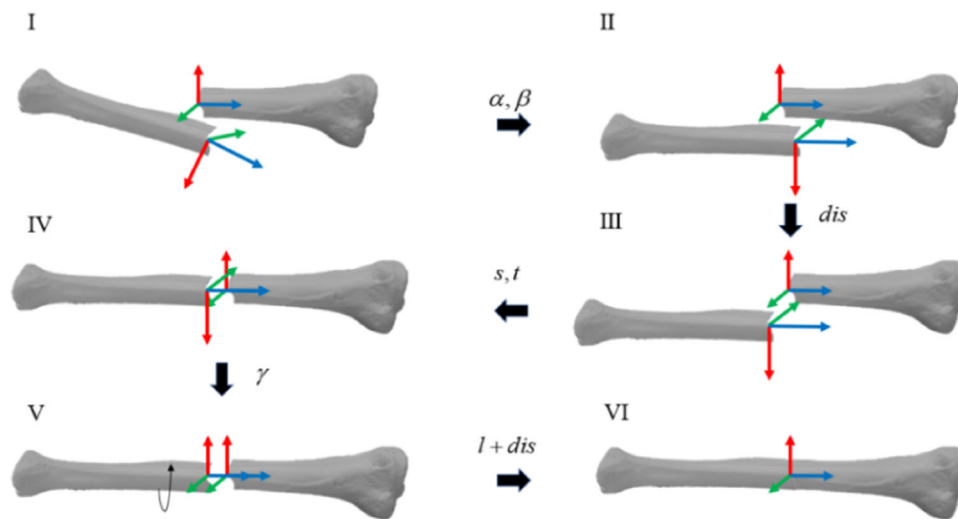


FIGURE 12 Schematic diagram of the fracture reduction process.

reduction path is collision-free. The specific implementation steps of the interosseous collision detection algorithm are as follows:

1. The fractured bone model reconstructed through VTK is stored in the data format of PolyData. Traverse the spatial points in the reconstructed distal bone PolyData data, and for each point, determine the inclusion relationship with the proximal bone PolyData polyhedral model using the priming ray method.
2. If the result of the judgment at the current point is inside the proximal bone model, the result is judged to be a collision, the algorithm loop is terminated, and the result is returned.
3. If the result at the current point is outside the proximal bone model, mark and find the next point to continue the inclusion relationship judgment until all the spatial points in the distal bone PolyData are judged and marked as outside the proximal bone model, then the result is no collision, terminate the algorithm and return the result.

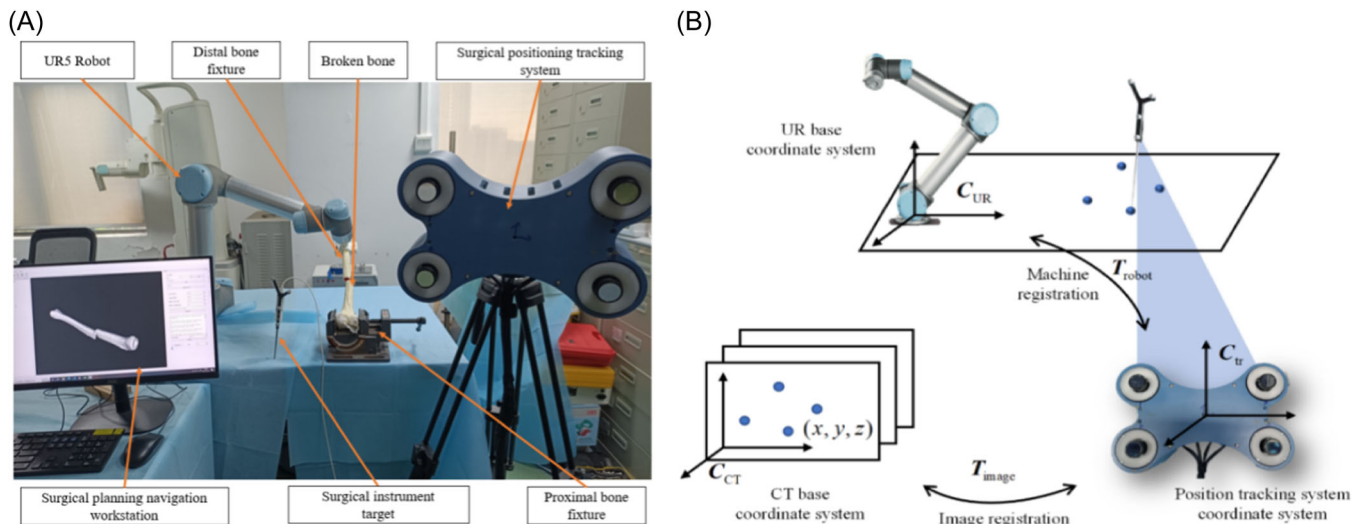


FIGURE 13 Fracture reduction surgery navigation system platform. (A) Hardware platform. (B) Conversion between coordinate systems.



FIGURE 14 Model bone. (A) Tibia model bone. (B) Model bone after amputation. (C) Distal bone jig and fixation.

TABLE 2 Reset planning parameter table.

Parameter type	Parameter value
Kd-tree search radius	4 mm
Long axis filter threshold	60°
Outlier statistics number range	50
Iterative closest point furthest registration range	25 mm
Planning step	2 mm

Figure 8 shows that when the algorithm is executed and the 172nd point is traversed, it is detected that the point is inside the proximal bone polyhedron model, indicating that a collision has occurred.

2.2.3 | Analysis of the reduction force of lower extremity fractures

In clinical fracture reduction surgery of the lower extremity, if the reduction is not performed properly, excessive force will be

applied to the local soft tissues, which will cause secondary damage to the soft tissues at the fracture site. To analyze the influence of the adjustment sequence of the reset parameters on the reset force, the open-source human skeletal muscle model 3Dgaint2392 provided by OpenSim is used, as shown in Figure 9A. As shown in Figure 9B, the skeletal muscle model is idealized to consist of multiple muscle-tendon units, and each unit is composed of a contraction unit (CE), a parallel unit (PE), and a series unit (SE).²⁶ The force of the skeletal muscle also corresponds to the sum of the active force of the muscle, the passive force of the muscle, and the force of the tendon.

Taking as an example a total translation of 5 mm and a total rotation of 20°, add a stretch of 20 mm, reset these parameters in different orders, and record the magnitude of the passive force on the muscle fibers during the reset process. The results are shown in Figure 10.

There are many clinical treatment methods, but they basically include preoperative diagnosis, stretching and traction, manual reduction, and fixation and recovery. If stretching and traction are performed directly without angle reduction, multiple muscles will generate large reduction forces due to torsional deviation, which is consistent with the results shown in Figure 10A.

FIGURE 15 Reset planning path visualization preview.

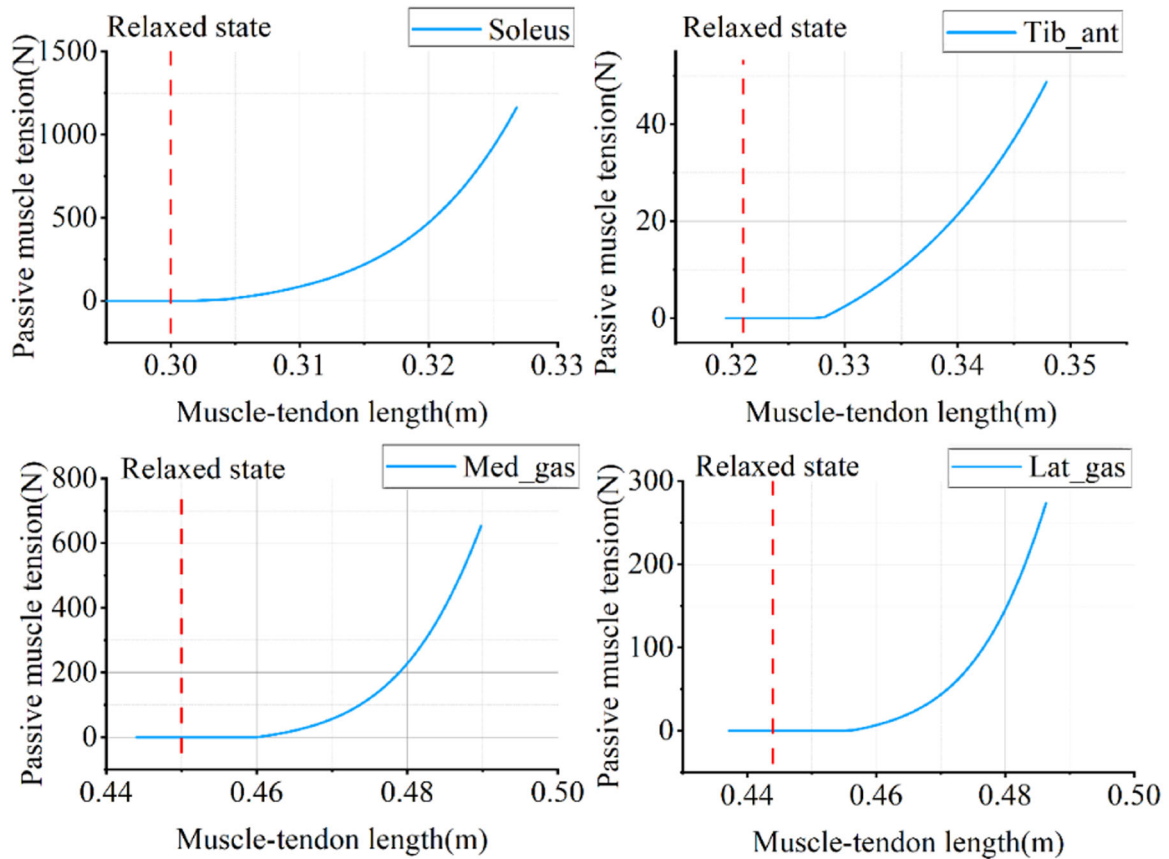
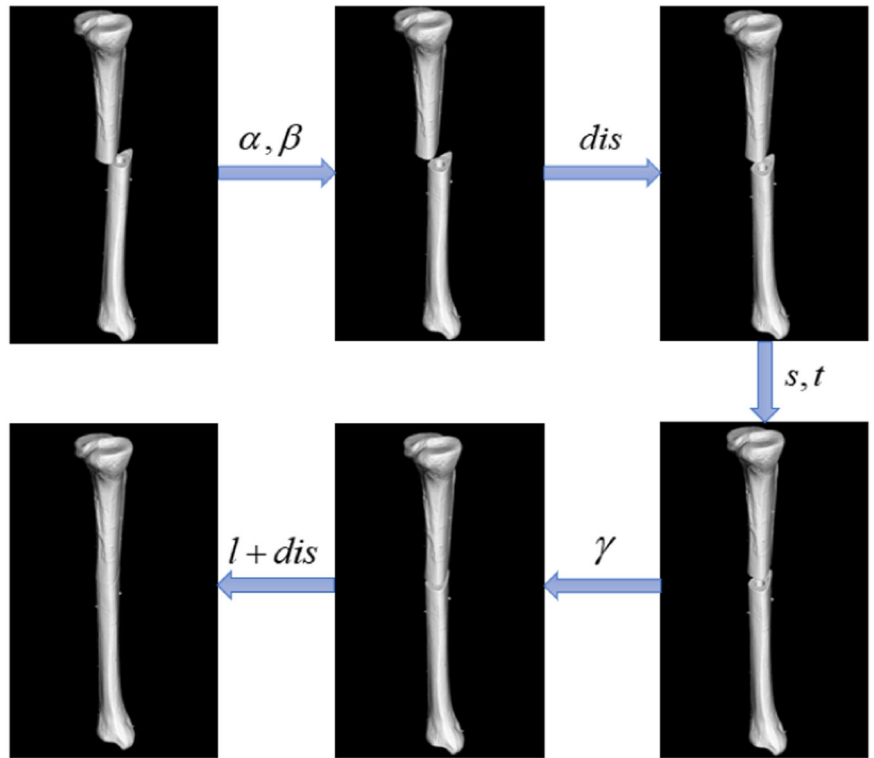


FIGURE 16 The relationship between passive force and length of each skeletal muscle.

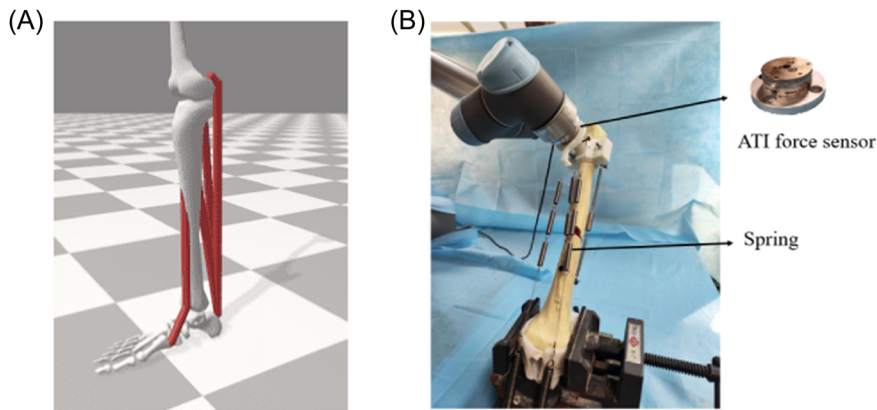


FIGURE 17 Muscle simulation for resetting force test. (A) Simulation of muscles using springs in the experiment. (B) Simulation of muscles using springs in the experiment.

2.2.4 | Algorithm design and integration of reset path planning

The reduction path planning should ensure that the fractured bones do not collide during the reduction process and minimize the reduction force during the entire reduction process. The reset path planning algorithm is shown in Figure 11. The actual reset process is to output in reverse order according to the planned coordinate transformation matrix sequence, and then perform pose transformation on the actual position of the distal bone. The actual reset process is shown in Figure 12.

3 | EXPERIMENTS

3.1 | Experimental setup

The experimental setup is shown in Figure 13A. It includes the surgical navigation workstation responsible for carrying the surgical planning and navigation software system, the multi-eye surgical instrument positioning and tracking system responsible for obtaining target pose information, and the surgical actuator responsible for the actual operation. As shown in Figure 13B, the system is integrated through image registration and machine registration.

3.2 | Lower extremity fracture reduction surgery experiment

In the experiment, a human tibia model made of polymeric materials was used to simulate the broken bone of a fractured patient, and steel balls with a diameter of 1 mm were attached to the model bone as feature points for registration. The model bone is truncated at the middle part of the bone in advance. A relative pose relationship is set between the two broken bones to simulate the situation of the patient after a fracture, and its CT image is scanned. The proximal bone is fixed on the test bench with a clamp, and the distal bone is fixed at the end of the robot for pose adjustment. The model bone is shown in Figure 14.

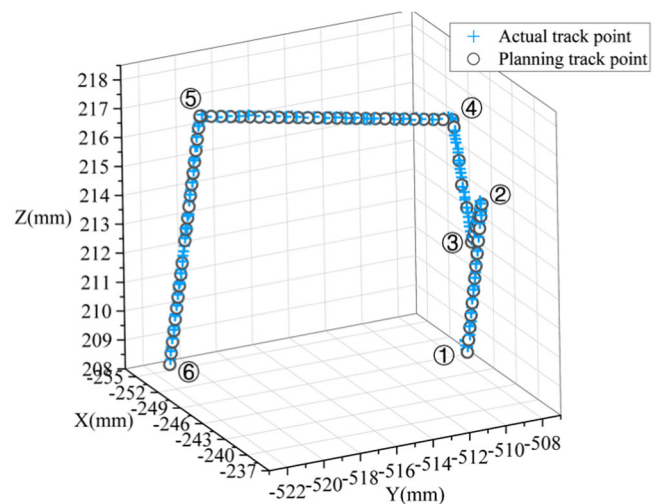


FIGURE 18 Actual reset path and planned reset path.

The whole experimental process is the same as the clinical fracture reduction surgery. First, the CT image is input, and image segmentation, 3D reconstruction and cross-sectional point cloud registration are sequentially performed. After the cross-sectional registration is completed, the reduction path is planned. After verifying that there is no abnormality in the planned path in the planning preview window, you can enter the planning results into the robot control plug-in to perform the reset. The reset parameters are shown in Table 2. Figure 15 shows the visualized preview result of the plan.

The reset path after the coordinate conversion is transmitted to the robot through the control plug-in, the reset operation is performed, and the actual position of the robot end positioning point is recorded in real time.

In terms of force analysis, an experiment was designed to simulate the muscle reset force at the fracture site to verify that the system's planned path for lower extremity fracture reduction can reduce the reset force during the reset process. Use OpenSim to analyze the relationship between the passive force of muscle fibers and the total length of muscle-tendon, as shown in Figure 16, simulate the main skeletal muscles near the fracture through

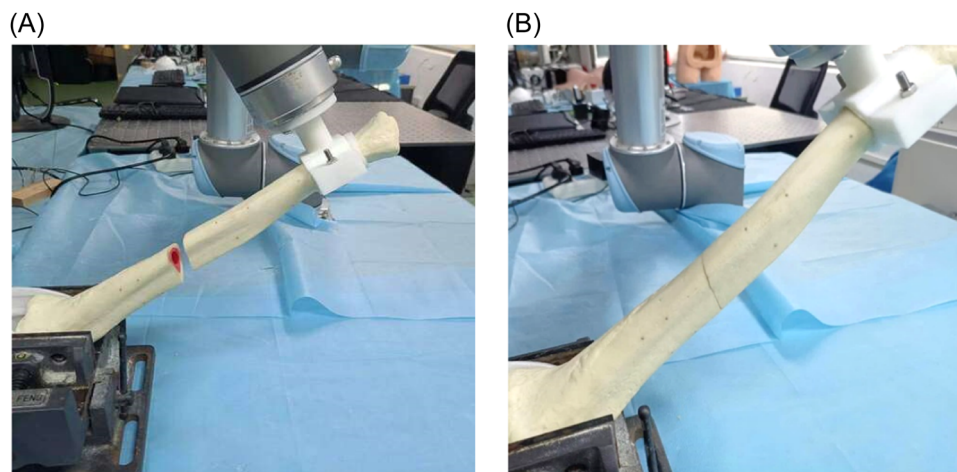


FIGURE 19 Model bone reduction effect. (A) Before fracture reduction. (B) After fracture reduction.

TABLE 3 Reset accuracy table.

Anchor group number	Error value (mm)
1	0.8637
2	0.9271
3	0.8946
4	0.8539

different spring combinations, and record the reset force under different reset paths to verify the reset planning method in this study effectiveness.

The total length of the muscle-tendon is stretched 0–20 mm compared to the relaxed state as a reference standard, Springs with different basic parameters are combined to simulate the stress state of each muscle. The screws are fixed by referring to the four skeletal muscle attachment points in the OpenSim model, as shown in Figure 17. An ATI force sensor is connected between the end of the robot and the distal bone fixture.

4 | RESULTS

In this experiment, the registration errors of image registration and machine registration were 0.2841 and 0.2934 mm, respectively, and the errors were within the normal range. In the above experiment, the actual position of the positioning point at the end of the robot was recorded, and the actual trajectory was compared with the planned trajectory. The results are shown in Figure 18.

As shown in Figure 18, the actual trajectory is basically the same as the system planning trajectory, and the reset process is successfully completed according to the planning result. Figure 19 shows the cross-section of the model bone before and after reduction. It can be seen that the reduction of the section is visually complete, and the section is well aligned.

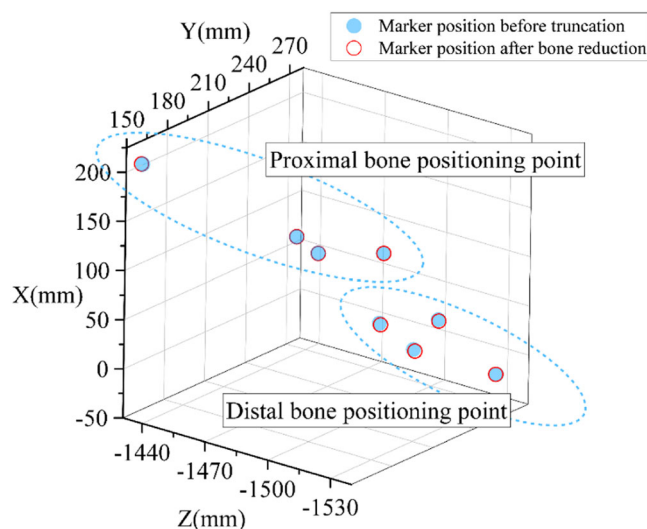


FIGURE 20 Position of anchor point before and after reset.

Before the model bone is amputated, the coordinate data of the steel ball on the model bone is stored by the optical positioning system. After, the reset is completed, the reset steel ball is positioned in the same order. To avoid the influence of measurement errors, the positioning data of 16 steel balls on the model bone were actually measured in the experiment, and finally, eight noncoplanar positioning points were randomly selected as a group for error calculation. A total of 4 groups were calculated. The reset accuracy results are shown in Table 3, and Figure 20 shows the positions of the first set of anchor points before and after resetting in 3D space.

It can be seen from the experimental results that the average error of the reduction of the model bone is within 1.0 mm, and the reduction results are good through discussions with cooperating clinicians. The visual reset condition is normal.

According to the experimental platform that simulates muscles, the reset process records the force in all directions of the ATI force sensor in real time. Then, a comparative test is performed, and the

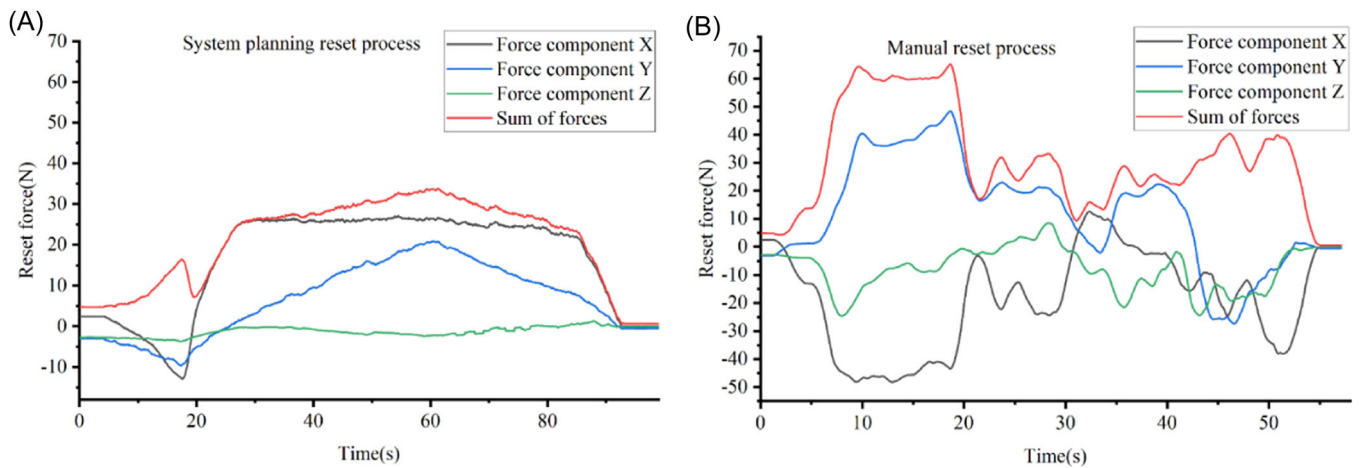


FIGURE 21 Resetting force change curve. (A) System planning reset process. (B) Manual reset process.

results of the two recorded forces and the resulting force calculations are shown in Figure 21.

It can be seen from the figure that the maximum reset force generated during the reset process can be significantly reduced by using the reset path planned above. At the same time, since the manual reduction process relies on vision and experience to align the cross-section, the angle is repeatedly fine-tuned in the later stage of reduction, and hand-shaking is unavoidable, so the reduction force fluctuates greatly, which may easily cause secondary damage to muscles and other soft tissues. The reset planning of the surgical navigation system can effectively avoid these situations.

5 | CONCLUSION

Aiming at the low precision of lower limb fracture reduction and secondary trauma easily generated during the reduction process, this study designs and implements a planning and navigation system for lower limb fracture reduction surgery.

First, the uniform point cloud model of the fractured bone was obtained by 3D reconstruction and uniform sampling of the fractured bone. On this basis, we innovatively proposed the bone long axis normal filtering method, which successfully realized the stable and reliable extraction of the point cloud of the distal bone and proximal bone sections. Then we completed the accurate point cloud alignment of the distal bone and proximal bone sections.

Then, in combination with clinical practice, the reduction parameters of lower extremity fractures were determined. A collision detection algorithm was designed and implemented for the reduction process of lower extremity fractures. At the same time, based on the analysis of the reduction force generated by the soft tissue near the fracture, a safe reduction path evaluation method based on the minimum reduction force was proposed. The reduction force path planning algorithm for lower extremity fractures can effectively reduce the intraoperative reduction force while ensuring accurate

reduction, thereby reducing secondary trauma during the reduction process.

Finally, the experimental platform for the planning and navigation system of lower limb fracture reduction surgery was built, and the lower limb fracture reduction surgery experiment and the reset force experiment were conducted. The feasibility and effectiveness of the system are verified.

AUTHOR CONTRIBUTIONS

Hanwen Du: Conceptualization; formal analysis; methodology; software; validation; visualization; writing—original draft; writing—review and editing. **Geyang Wu:** Conceptualization; formal analysis; methodology; software; visualization; writing—review and editing. **Ying Hu:** Conceptualization; resources; supervision; writing—review and editing. **Yucheng He:** Conceptualization; formal analysis; methodology; resources; supervision; validation; writing—review and editing. **Peng Zhang:** Conceptualization; supervision; validation; writing—review and editing.

ACKNOWLEDGMENTS

The authors would like to thank the Cognitive and Interactive Technologies Research Center for making this study possible. This study was supported by Guangdong Basic and Applied Basic Research Foundation (2022A1515010574), Shenzhen Science and Technology Program (JCYJ20210324101012031), Shenzhen Basic Research (JCYJ20220818101412026), Regional Joint Fund of Guangdong (2021B1515130003), and Shenzhen Key Laboratory of Minimally Invasive Surgical Robotics and System (ZDSYS201707271637577).

CONFLICT OF INTEREST STATEMENT

The authors declare no conflict of interest.

DATA AVAILABILITY STATEMENT

The data that support the findings of this study are available on request from the corresponding authors. This article does not involve any private data.

TRANSPARENCY STATEMENT

The lead author Yucheng He, Peng Zhang affirms that this manuscript is an honest, accurate, and transparent account of the study being reported; that no important aspects of the study have been omitted; and that any discrepancies from the study as planned (and, if relevant, registered) have been explained.

ORCID

Hanwen Du  <http://orcid.org/0009-0004-0434-9602>

Yucheng He  <http://orcid.org/0000-0001-8592-5480>

REFERENCES

- Wang M, Li D, Shang X, Wang J. A review of computer-assisted orthopaedic surgery systems. *Int J Med Robot Comput Assist Surg.* 2020;16:1-28.
- Lee C-C, Jung KH, Lee KJ, Park KB. A bibliometric analysis of the field of computer-assisted orthopedic surgery during 2002-2021. *Clin Orthop Surg.* 2023;15:227-233.
- Ewurum CH, Guo Y, Pagnha S, Feng Z, Luo X. Surgical navigation in orthopedics: workflow and system review. *advances in experimental medicine and biology.* *Intell Orthopaed.* 2018;1093:47-63.
- Lim S, Ha J, Yoon S, et al. Augmented reality assisted surgical navigation system for epidural needle intervention. *2021 43rd Annual International Conference of the IEEE Engineering in Medicine & Biology Society (EMBC).* Guadalajara, Mexico. IEEE; 2021:4705-4708.
- Cao Y, Liu Z, Yu H, Hong W, Xie L. Spatial shape sensing of a multisection continuum robot with integrated DTG sensor for maxillary sinus surgery. *IEEE/ASME Trans Mechatron.* 2023;28:715-725.
- Ferrero E, Mazda K, Simon AL, Ilharreborde B. Preliminary experience with SpineEOS, a new software for 3D planning in AIS surgery. *Eur Spine J.* 2018;27:2165-2174.
- Knez D, Likar B, Pernus F, Vrtovec T. Computer-assisted screw size and insertion trajectory planning for pedicle screw placement surgery. *IEEE Trans Med Imaging.* 2016;35:1420-1430.
- Qi X, Meng J, Li M, et al. An automatic path planning method of pedicle screw placement based on preoperative CT images. *IEEE Trans Med Robot Bion.* 2022;4:403-413.
- Miura M, Hagiwara S, Nakamura J, Wako Y, Kawarai Y, Ohtori S. Interobserver and intraobserver reliability of computed tomography-based three-dimensional preoperative planning for primary total knee arthroplasty. *J Arthroplasty.* 2018;33:1572-1578.
- Gao L, Ding K, Liu J, et al. Design and development of a knee surgery planning system. *2020 Chinese Control and Decision Conference (CCDC), Hefei, China.* IEEE; 2020:2053-2059.
- Sugano N. *Computer Assisted Orthopaedic Surgery for Hip and Knee.* Springer; 2018:105-118.
- Fürnstahl P, Székely G, Gerber C, Hodler J, Snedeker JG, Harders M. Computer assisted reconstruction of complex proximal humerus fractures for preoperative planning. *Med Image Anal.* 2012;16:704-720.
- Han R, Uneri A, Vijayan R, et al. Fracture reduction planning and guidance in orthopaedic trauma surgery via multi-body image registration. *Med Image Anal.* 2021;68:101917.
- Zhao C, Wang Y, Wu X, Zhu G, Shi S. Design and evaluation of an intelligent reduction robot system for the minimally invasive reduction in pelvic fractures. *J Orthop Surg Res.* 2022;17:205.
- Liu P, Hewitt N, Shadid W, Willis A. A system for 3D reconstruction of comminuted tibial plafond bone fractures. *Comput Med Imaging Graph.* 2021;89:101884.
- Lee S, Joung S, Ha HG, et al. 3D image-guided robotic system for bone fracture reduction. *IEEE Robot Autom Lett.* 2022;7:4353-4360.
- Du H, Hu L, Li C, He C, Zhang L, Tang P. Preoperative trajectory planning for closed reduction of long-bone diaphyseal fracture using a computer-assisted reduction system. *Int J Med Robot Comput Assist Surg.* 2015;11:58-66.
- Fu Z, Sun H, Dong X, et al. Indirect visual guided fracture reduction robot based on external markers. *Int J Med Robot Comput Assist Surg.* 2021;17:1-11.
- Buschbaum J, Fremd R, Pohlemann T, Kristen A. Introduction of a computer-based method for automated planning of reduction paths under consideration of simulated muscular forces. *Int J Comput Assist Radiol Surg.* 2017;12:1369-1381.
- Xiao D, Lian C, Deng H, et al. Estimating reference bony shape models for orthognathic surgical planning using 3D point-cloud deep learning. *IEEE J Biomed Health Inform.* 2021;25:2958-2966.
- Boutillon A, Salhi A, Burdin V, Borotikar B. Anatomically parameterized statistical shape model: explaining morphometry through statistical learning. *IEEE Trans Biomed Eng.* 2022;69:2733-2744.
- Sun X, Wang H, Wang W, et al. A statistical model of spine shape and material for population-oriented biomechanical simulation. *IEEE Access.* 2021;9:155805-155814.
- Otsu N. A threshold selection method from gray-level histograms. *IEEE Trans Syst Man Cybern.* 1979;9:62-66.
- Falcão AX, Udupa JK, Samarasekera S, Sharma S, Hirsch BE, Lotufo RA. User-steered image segmentation paradigms: live wire and live lane. *Graph Models Image Process.* 1998;60:233-260.
- Wang J, Huang Z, Yang X, Jia W, Zhou T. Three-dimensional reconstruction of jaw and dentition CBCT images based on improved marching cubes algorithm. *Procedia CIRP.* 2020;89:239-244.
- Mo F, Li F, Behr M, Xiao Z, Zhang G, Du X. A lower limb-pelvis finite element model with 3D active muscles. *Ann Biomed Eng.* 2018;46:86-96.

How to cite this article: Du H, Wu G, Hu Y, He Y, Zhang P. Experimental research based on robot-assisted surgery: lower limb fracture reduction surgery planning navigation system. *Health Sci Rep.* 2024;7:e2033. doi:10.1002/hsr2.2033